

Distance-Weighted Kalman Fusion for Precise Docking Problems

Claus Lenz¹, Thorsten Röder¹, Markus Rickert², Alois Knoll¹

¹Robotics and Embedded Systems, Department of Informatics, Technische Universität München

²Cyber-Physical Systems, fortiss

Abstract—This paper proposes a way to solve a highly precise docking problem for a flexible delivery in production environments. The docking problem is seen as one of the fundamental problems to enable more flexible automation using mobile robots. A non-holonomic differential-driven robot with two conveyor belts is used to deliver boxes with goods to two docking slots on an assembly belt and unload them precisely. In order to localize the robot in front of the docking slots, a safety LIDAR and two “minimal invasive” reflecting markers are used that are completely light invariant, thus reaching industrial robustness. This measurement is fused with odometry using a Kalman filter and a distance weighted way to compute the reliability of the data streams.

I. INTRODUCTION

Many industrial facilities already have employed exhaustive methods optimizing productivity in their production labs and construction assemblies [1], [2], [3]. In contrast to traditional optimization methods, the potential of mobile service robotics can be seen as a next revolution with respect to further optimization potentials [4]. This is especially true in conjunction with the increasing demand for flexibility in product and supply management, environmental changes or highly dynamical production flows [5]. As the mobile service robotics can be one solution for further optimizations, the overall performance and robustness is still improvable in real life applications although impressive work was for example done in [6], [7].

A mobile robot requires robust basic capabilities like self-localization, navigation, and closed loop control in order to fulfill given mobility tasks. Besides the overall robustness and reliability of these functionalities, non-functional requirements must also be met for serious industrial usage including smoothness of actuator control, speed, and energy optimizations efficiency, and a safe and predictable behavior of the mobile robot. Fundamental constraints are typically given by choosing a mobile platform of holonomic or non-holonomic type, each with its own advantages and disadvantages.

In this paper, we propose a methodology for solving a highly precise docking problem. The docking problem is one of the fundamental problems such as the handover of goods or the battery charging [8], [9], [10], [11], [12]. Approaches for the docking problem typically use optical, IR [13], or electromagnetic [14], [15] markers. Opposite to the docking in charging positions, the presented application example in this paper requires highly precise approaching. Here, two conveyor belts mounted on a mobile robot are

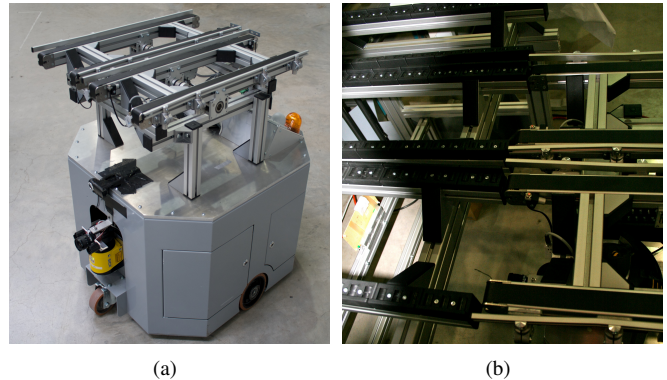


Fig. 1. (a) The differential-driven platform used in this work. It is equipped with a LIDAR, several cameras and two conveyor belts to load, carry, and unload boxes on assembly line docking station as depicted in (b).

used to deliver boxes with goods to two docking slots on an assembly belt. These boxes need to be precisely pushed from the robot in order to glide into the docking slot. Using a non-holonomic differential-driven platform, this approach needs to be precomputed exactly and the corresponding path-following needs to be precise as well.

In order to localize the robot in front of the docking slots, we make use of the already installed safety LIDAR and two reflecting markers. This way, almost no invasive markers need to be added and the results are completely light invariant, thus reaching industrial robustness. This measurement is fused with odometry using a Kalman filter [16] and a distance weighted way to compute the reliability of the data streams.

The paper is organized as follows: Sect. II introduces the differential kinematics of the mobile robot, Sect. III describes how a given path can be smoothly followed with such a kinematic, Sect. IV explains the localization and the fusion method in detail and overviews the results.

II. DIFFERENTIAL-DRIVEN MOBILE PLATFORM

A differential-driven robot—such as the one depicted in Fig. 1—is controlled via two independently actuated wheels on a common axis that have a distance of $2b$ from each other. The robot can move with the linear velocity u and the angular velocity ω along the body axes (Fig. 2). With the assumption that the wheels are perfectly rolling, the kinematic model of

such a robot can be expressed as:

$$u = \frac{1}{2}(v_r + v_l) \quad (1)$$

$$\omega = \frac{1}{2b}(v_r - v_l), \quad (2)$$

where the maximal velocities of the wheels are bound to certain limit values V_m , e.g., due to hardware limits of the motors.

Without any other limitation, such a robot can drive on paths with arbitrary curvatures

$$\kappa = \frac{1}{b} \frac{v_r - v_l}{v_r + v_l}. \quad (3)$$

The curvature κ of a planar path is related to the radius r_c of a circle that most closely approximates the path at a given point (P):

$$\kappa = \frac{1}{r_{c(P)}}. \quad (4)$$

This means, that for counter-rotating motors, the curvature becomes infinite and the robot turns on the spot.

While the robot is driving on the ground plane in a two-dimensional space (x and y), the curvature κ is one-dimensional. Therefore, for arbitrary plane paths that can be expressed parametrically by $(x(t), y(t))$, the signed curvature is given by

$$\kappa = \frac{\dot{x}\ddot{y} - \dot{y}\ddot{x}}{(\dot{x}^2 + \dot{y}^2)^{\frac{3}{2}}}. \quad (5)$$

This equation can be reduced to

$$\kappa = \frac{\ddot{y}}{(1 + \dot{y}^2)^{\frac{3}{2}}} \quad (6)$$

$$= \frac{f''(x)}{(1 + f'(x)^2)^{\frac{3}{2}}}, \quad (7)$$

under the assumption $\dot{x} = 1$ and $\ddot{x} = 0$.

The curvature [17] is the central parameter of robotic motion when considering maximization of linear velocity and minimization of snatchyness. However, a smooth behavior of a mobile robot without hard brakes is desirable due to multiple issues: From an energy efficiency point of view, hard brakes should be avoided. Additionally, smooth—and therefore predictable—behavior of the robot increases safety, as humans can estimate the trajectory and act accordingly.

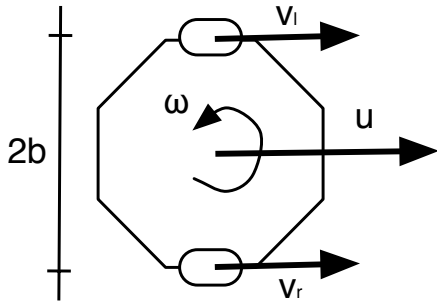


Fig. 2. Differential-driven platforms with a wheelbase of $2b$ are controlled by the turning velocities v_l and v_r of the wheels, resulting in a linear velocity u and an angular velocity ω

Hence, if we want to apply this strategy, the motor velocities should always remain positive

$$v_l, v_r \in [0, V_m], \quad (8)$$

and the curvature of the reference path needs to stay bounded [18] to

$$\kappa = \left[-\frac{1}{b}, \frac{1}{b} \right]. \quad (9)$$

III. PATH FOLLOWING

If we constrain κ , we will get a smoother path trajectory $l \in \mathbb{R}^P$, that can be followed if the robot controller takes special care of a) the distance between the robot and the path and b) the angle between the forward velocity vector and the tangent to the path. Both should be reduced to zero [19] to follow the path.

Following [20], the path following problem can be explained in more detail: Let $P = (x_P, y_P)$ be an arbitrary point on the path l and $Q = (x_Q, y_Q)$ be the center of mass¹ of the differential-driven robot. Along the path, a tangential reference frame $\{F\}$ is attached at every point with a signed curvilinear abscissa denoted with s . This tangential reference system can be referred to as Serret-Frenet frame. Thus, the position of the robot Q can be described in the inertial reference frame $\{I\}$ as

$$\mathbf{q}^I = [x_Q \quad y_Q \quad 0]^T \quad (10)$$

and in $\{F\}$ as

$$\mathbf{q}^F = \mathbf{r} \quad (11)$$

$$= [s_{1Q} \quad y_{1Q} \quad 0]^T. \quad (12)$$

Equivalently, P is given in $\{I\}$ as

$$\mathbf{p}^I = [x_P \quad y_P \quad 0]^T \quad (13)$$

and in $\{F\}$ always as

$$\mathbf{p}^F = [0 \quad 0 \quad 0]^T. \quad (14)$$

The rotation from $\{I\}$ to $\{F\}$ is given by $\mathbf{R}_{I,F} = \mathbf{R}(\theta_c)$, parametrized by the angle θ_c between the inertial frame $\{I\}$ and the curvilinear abscissa s . The reverse rotation is respectively given by $\mathbf{R}_{F,I} = \mathbf{R}^{-1}(\theta_c)$.

The angular velocity is defined by

$$\omega_c = \dot{\theta}_c \quad (15)$$

$$= \kappa_r(s) \dot{s}, \quad (16)$$

with $\kappa_r(s)$ being the curvature of the reference path.

Using these definitions, the velocities of both points Q and P can be easily expressed in both systems.

$$\dot{\mathbf{p}}^F = \mathbf{R}_{I,F} \dot{\mathbf{p}}^I \quad (17)$$

$$= [\dot{s} \quad 0 \quad 0]^T \quad (18)$$

The velocity of point Q in $\{I\}$ is given by

$$\dot{\mathbf{q}}^I = [\dot{x}_Q \quad \dot{y}_Q \quad 0]^T \quad (19)$$

$$= \dot{\mathbf{p}}^I + \mathbf{R}_{F,I} \dot{\mathbf{r}} + \mathbf{R}_{F,I} (\omega_c \times \mathbf{r}), \quad (20)$$

with \mathbf{r} being the vector from P to Q .

¹for the F5 this is also the center of rotation

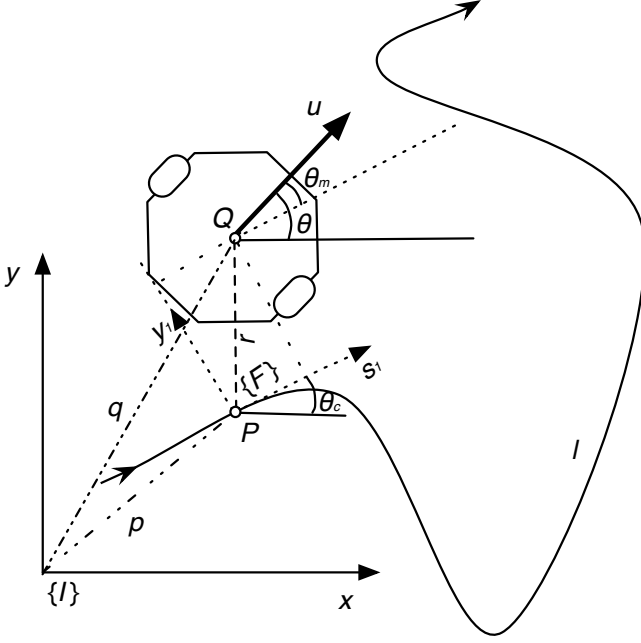


Fig. 3. The mobile robot should follow a given path l . Its position is expressed in an inertial frame I and a Frenet frame F rooted in the tangent space of the path. If the angle Θ_m and the distance between robot and path are reduced to zero, the robot moves on the given path

Now, the velocity of Q in $\{I\}$ can be expressed in $\{F\}$ by multiplying both sides with $\mathbf{R}_{I,F}$

$$\begin{aligned} \dot{\mathbf{q}}^F &= \mathbf{R}_{I,F} \dot{\mathbf{q}}^I \\ &= \dot{\mathbf{p}}^F + \dot{\mathbf{r}} + (\omega_c \times \mathbf{r}), \end{aligned} \quad (21)$$

with $\dot{\mathbf{r}} = [\dot{s}_{1Q} \ \dot{y}_{1Q} \ 0]^T$.

Considering the relation

$$\begin{aligned} \omega_c \times \mathbf{r} &= \begin{bmatrix} 0 \\ 0 \\ \kappa_r(s)\dot{s} \end{bmatrix} \times \begin{bmatrix} s_{1Q} \\ y_{1Q} \\ 0 \end{bmatrix} \\ &= \begin{bmatrix} -\kappa_r(s)\dot{s}y_{1Q} \\ \kappa_r(s)\dot{s}s_{1Q} \\ 0 \end{bmatrix}, \end{aligned} \quad (22)$$

equation (21) can be expressed as

$$\dot{\mathbf{q}}^F = \begin{bmatrix} \dot{s}(1 - \kappa_r(s)y_{1Q}) + s_{1Q} \\ y_{1Q} + \kappa_r(s)\dot{s}s_{1Q} \\ 0 \end{bmatrix} \quad (24)$$

and be solved for

$$\dot{s}_{1Q} = [\cos \theta_c \ \sin \theta_c] \begin{bmatrix} \dot{x}_Q \\ \dot{y}_Q \end{bmatrix} - \dot{s}(1 - \kappa_r(s)y_{1Q}) \quad (25)$$

$$\dot{y}_{1Q} = [-\sin \theta_c \ \cos \theta_c] \begin{bmatrix} \dot{x}_Q \\ \dot{y}_Q \end{bmatrix} - \kappa_r(s)\dot{s}s_{1Q}. \quad (26)$$

Applying the body-axis speed u (linear velocity), the yaw angle of the vehicle θ_m , and the respective angular velocity $\omega = \omega_m = \dot{\theta}_m$ together with the relationship

$$\begin{bmatrix} \dot{x}_Q \\ \dot{y}_Q \end{bmatrix} = u \begin{bmatrix} \cos \theta_m \\ \sin \theta_m \end{bmatrix} \quad (27)$$

and the mathematical rules for $\theta = \theta_m - \theta_c$

$$\cos \theta = \cos \theta_m \cos \theta_c + \sin \theta_m \sin \theta_c \quad (28)$$

$$\sin \theta = \sin \theta_m \cos \theta_c + \cos \theta_m \sin \theta_c, \quad (29)$$

the kinematic model of the unicycle robot can be expressed in $\{F\}$ as

$$\dot{s}_{1Q} = -\dot{s}(1 - \kappa_r(s)y_{1Q}) + u \cos \theta \quad (30)$$

$$\dot{y}_{1Q} = -\kappa_r(s)\dot{s}s_{1Q} + u \sin \theta \quad (31)$$

$$\dot{\theta} = \omega_m - \kappa_r(s)\dot{s}. \quad (32)$$

Recalling the problem formulation stated previously, a given path is followed exactly if s_{1Q} , y_{1Q} , and θ are zero. On the kinematic level, a locally positive-definite Lyapunov candidate function such as

$$V_1 = \frac{1}{2}(s_{1Q}^2 + y_{1Q}^2) + \frac{1}{\gamma}(\theta - \delta(y_{1Q}, u))^2 \quad (33)$$

can be applied [19] to proof the stability of the system, where it is assumed that

- $\lim_{t \rightarrow \infty} u(t) \neq 0$
- $\delta(0, u) = 0$
- $y_{1Q} u \sin \delta(y_{1Q}, u) \leq 0, \forall y \forall u$.

By choosing

$$\dot{\theta} = \delta - \gamma y_{1Q} u \frac{\sin \theta - \sin \delta}{\theta - \delta} - k_2(\theta - \delta) \quad (34)$$

$$\dot{s} = u \cos \theta + k_1 s_{1Q}, \quad (35)$$

with $k_1 > 0$ and $k_2 > 0$ being non-negative constants, the time derivative follows

$$\dot{V}_1 = -k_1 s_{1Q}^2 - \frac{1}{\gamma}(\theta - \delta)^2 + y_{1Q} u \sin \delta \leq 0 \quad (36)$$

and guarantees that all state variables remain bounded [20]. The function δ has the purpose of shaping the transient convergence of the state to zero and can be chosen according to specific design demands.

Now, (1), (2), (32), and (35) can be merged together, resulting in

$$v_r = u + b(\kappa_r \dot{s} + \dot{\theta}) \quad (37)$$

$$v_l = u - b(\kappa_r \dot{s} + \dot{\theta}). \quad (38)$$

A further combination of these equations with (3) results in the closed loop curvature of the robot

$$\kappa_{cl} = \frac{\kappa_r \dot{s} + \dot{\theta}}{u}, \quad (39)$$

for which can be shown [18] that

$$\lim_{t \rightarrow \infty} \kappa_{cl} = \kappa_r \quad (40)$$

if the path-following error tends to zero. Please refer to Fig. 4 for an example where the closed loop curvature converges to the reference curvature as the robot follows the path.

Keeping this in mind, the proposed strategy for keeping the robot on a given path becomes

$$u = \begin{cases} \frac{1}{2}V_m & , \text{ if } V_1 \geq \epsilon \\ \frac{1}{1+b|\kappa_r(s)|}V_m & , \text{ if } V_1 < \epsilon \end{cases} \quad (41)$$

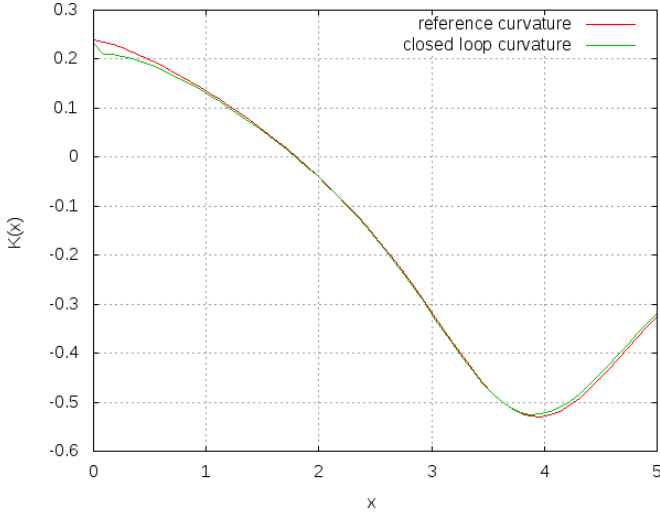


Fig. 4. Example path where the closed loop curvature converges to the reference curvature as the robot follows the path

for the linear velocity with $\epsilon > 0$ being a threshold value regulating the path following error and

$$\omega = \dot{\theta} + \kappa_r(s)\dot{s} \quad (42)$$

for the angular velocity.

IV. DOCKING PROBLEM

To follow a given path, it is necessary to localize the robot and to keep track of its position to minimize the path-following error. We make use of the safety LIDAR that is already attached to the robot and detect two reflecting markers (left and right) in the polar coordinate frame of the LIDAR: $P_L^{\text{pol}} = (r_L, \theta_L)$, and $P_R^{\text{pol}} = (r_R, \theta_R)$. Please refer to Fig. 5 for a schematic view. These two points are projected to the Cartesian coordinate frame of the robot:

$$P_L = (r_L \cos \theta_L, r_L \sin \theta_L) \quad (43)$$

$$P_R = (r_R \cos \theta_R, r_R \sin \theta_R). \quad (44)$$

With these points, we can compute

$$\beta = \cos^{-1} \left(\frac{|P_M - P_R|^2 + |P_M|^2 - |P_R|^2}{2|P_M - P_R||P_M|} \right), \quad (45)$$

which can directly be used to express the angular position of the robot

$$\alpha = \tan^{-1} \left(\frac{P_{L,x} - P_{R,x}}{P_{L,y} - P_{R,y}} \right). \quad (46)$$

The point between these two points in the middle of the docking slot

$$P_M = \frac{1}{2}(P_L + P_R) \quad (47)$$

is the center of the coordinate frame in which we want to estimate the robot's position. If we use this as center for a polar coordinate frame, we can interpret β as the angle and $d_m = |P_M|$ as the length. This can also be transformed to a Cartesian coordinate frame which results in

$$P_{\text{robot}} = (d_m \cos \beta, d_m \sin \beta). \quad (48)$$

Hence, the final result of the measurement is given by

$$\hat{p}_l = (P_{\text{robot},x}, P_{\text{robot},y}, \alpha)^T \quad (49)$$

$$= (\hat{x}_l, \hat{y}_l, \hat{\alpha}_l)^T. \quad (50)$$

Additionally, the odometry data is initialized with the first measurement of the LIDAR and then propagated ($\hat{p}_o = (\hat{x}_o, \hat{y}_o, \hat{\alpha}_o)^T$) using the wheel-diameter and the kinematic model.

Because the measuring directly returns the position and orientation of the robot with respect to the goal position, we can work in this space and comply with the linearity and Gaussian requirements of a Kalman filter [21]. The robot dynamics and the measurement model are given by

$$\mathbf{x}_t = (x, y, \alpha, \dot{x}, \dot{y}, \dot{\alpha})^T \quad (51)$$

$$= \mathbf{F}_t \mathbf{x}_{t-1} + \mathbf{B}_t \mathbf{w}_t \quad (52)$$

and

$$\mathbf{z}_t = (\hat{x}_l, \hat{y}_l, \hat{\alpha}_l, \hat{x}_o, \hat{y}_o, \hat{\alpha}_o)^T \quad (53)$$

$$= \mathbf{H}_t \mathbf{x}_t + \mathbf{C}_t \mathbf{v}_t. \quad (54)$$

\mathbf{w}_t and \mathbf{v}_t are zero-mean, white Gaussian noise variables, with covariance matrices $\mathbf{W}_t, \mathbf{V}_t$ respectively. We are using a constant velocity model with white noise acceleration (WNA)

$$\mathbf{F}_t = \begin{bmatrix} \mathbf{I}_{3 \times 3} & \mathbf{I}_{3 \times 3} \delta t \\ 0 & \mathbf{I}_{3 \times 3} \end{bmatrix}, \quad \mathbf{B}_t = \begin{bmatrix} \frac{1}{2} \mathbf{B}_0 \delta t^2 \\ \mathbf{B}_0 \delta t \end{bmatrix} \quad (55)$$

and

$$\mathbf{H}_t = \begin{bmatrix} \mathbf{I}_{3 \times 3} \\ \mathbf{I}_{3 \times 3} \end{bmatrix} \quad (56)$$

for the measurement Jacobian.

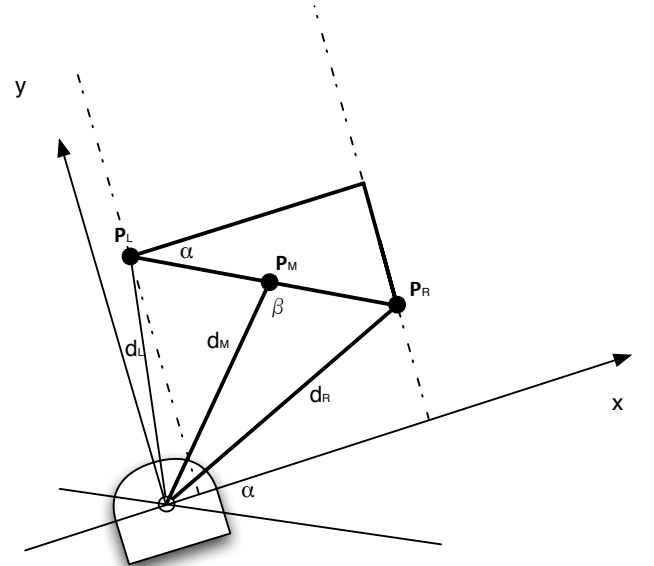


Fig. 5. Schematic view to geometrically solve the position and angle of the mobile robot using a LIDAR and two markers

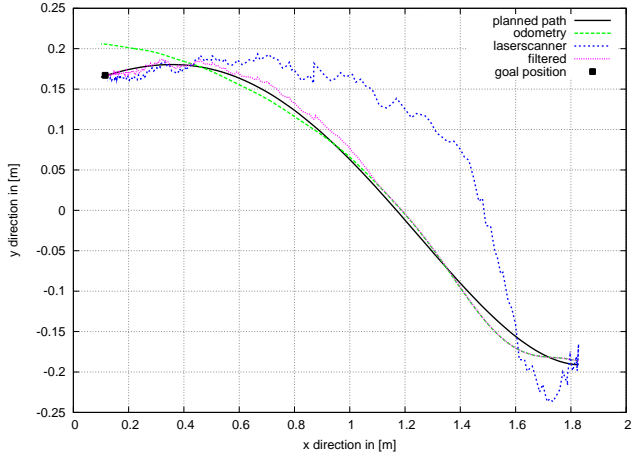


Fig. 6. Docking of the robot to the right assembly line position. The purple line is the fusion of the odometry data (green) and the LIDAR measurements (blue)

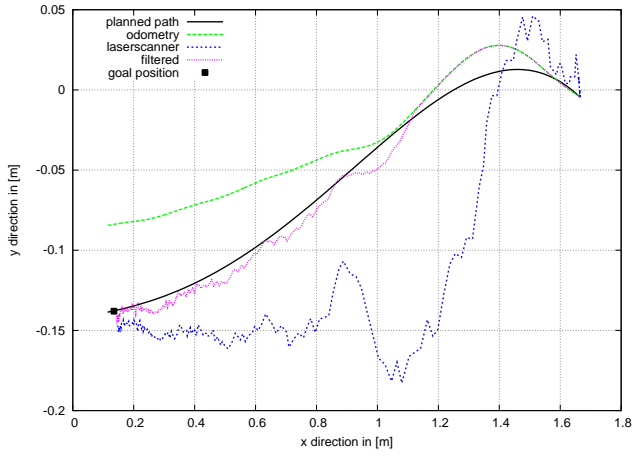


Fig. 7. Docking of the robot to the left assembly line position. The purple line is the fusion of the odometry data (green) and the LIDAR measurements (blue)

The overall noise covariance matrices

$$\mathbf{Q}_t = \mathbf{B}_t \mathbf{W}_t \mathbf{B}_t^T \quad (57)$$

$$\mathbf{R}_t = \mathbf{C}_t \mathbf{V}_t \mathbf{C}_t^T, \quad (58)$$

with \mathbf{R} being a diagonal matrix, realize the optimal Bayesian predictor-corrector scheme by

$$\mathbf{x}_t^- = \mathbf{F}_t \mathbf{x}_{t-1} \quad (59)$$

$$\mathbf{P}_t^- = \mathbf{F}_t \mathbf{P}_{t-1}^- \mathbf{F}_t^T + \mathbf{Q}_t \quad (60)$$

and

$$\mathbf{x}_t = \mathbf{x}_t^- + \mathbf{K}_t (z_t - \mathbf{H}_t \mathbf{x}_t^-) \quad (61)$$

$$\mathbf{P}_t = (\mathbf{I} - \mathbf{K}_t \mathbf{H}_t) \mathbf{P}_t^-, \quad (62)$$

with the Kalman gain

$$\mathbf{K}_t = \mathbf{P}_t^- \mathbf{H}_t^T (\mathbf{H}_t \mathbf{P}_t^- \mathbf{H}_t^T + \mathbf{R}_t)^{-1}. \quad (63)$$

The two modalities used (LIDAR and odometry) show different behaviors with respect to the distance to the goal:

the odometry delivers smooth results, but if the initialization or the initial localization was not done properly, the error will be accumulated with the inherent drift in odometry data leading to an incorrect behavior. Opposite to that, the LIDAR localization method measures with a lot of noise, which reduces as the robot approaches the goal. Therefore, we use the noise covariance matrix to control the trust in the two signals by integrating the distance related variable d_t in order to update the matrix

$$\mathbf{R}_t(d_t) = \text{diag} \left[\begin{array}{c} \frac{1}{((1-a)+a(\frac{d_{max}-d_t}{d_{max}})) r_l} \\ \frac{1}{((1-a)+a(\frac{d_{max}-d_t}{d_{max}})) r_l} \\ \frac{1}{((1-a)+a(\frac{d_{max}-d_t}{d_{max}})) r_l} \\ \frac{1}{((1-b)+b(\frac{d_t}{d_{max}})) r_o} \\ \frac{1}{((1-b)+b(\frac{d_t}{d_{max}})) r_o} \\ \frac{1}{((1-b)+b(\frac{d_t}{d_{max}})) r_o} \end{array} \right], \text{ if } d_t < d_{max} \quad (64)$$

in each time step, with r_l and r_o being the initial inverse covariance values, a and b being splitting factor to guarantee a constant base value, and d_{max} representing the threshold when to apply the distance weighting of the matrix. If $d_t > d_{max}$, the initial values r_l and r_o are applied.

As it can be seen in Fig. 6 and Fig. 7, the proposed method was successfully applied in order to perform a docking maneuver. From an initial position in about 1.6m from the actual goal position, the robot was approaching to the two delivery positions of the docking station via a computed fourth-order polynomial trajectory. The robot is moving from right to left. With a predominance on the smooth odometry data in the beginning, the more and more accurate LIDAR measurement gets integrated. Throughout the approach, the planned path is being followed by the robot. Screenshots from the docking maneuver are depicted in Fig. 8.

V. CONCLUSIONS

In this paper, we have shown a way to precisely dock to an assembly line with a non-holonomic differential-driven mobile platform. The platform was equipped with two conveyor belts in order to carry boxes and unload them to a docking slot on an assembly line. To drive smoothly, the motion space was constraint to only positive motor velocities. The path to approach the goal position was computed using a fourth-order polynomial equation and followed using Frenet frame representations. To localize the robot, the safety LIDAR was used to detect two reflecting markers. This measurement was fused with a Kalman filter to determine the current position of the robot, that was used to control the robot on the path. The two modalities from odometry and the LIDAR were fused using a distance weighted way in order to compute the overall measurement noise covariance matrix that was used to compute the Kalman gain. The results in Sect. IV showed that a precise docking was possible and the loading and unloading could be performed successfully.

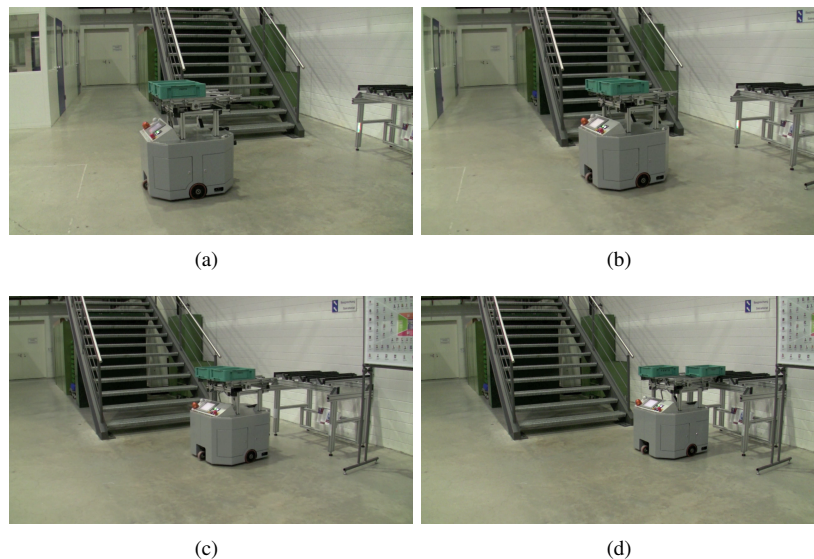


Fig. 8. Application scenario – The mobile platform F5 is approaching a docking station and delivers precisely two boxes.

VI. ACKNOWLEDGMENTS

This work was partially supported by the DFG excellence initiative research cluster *CoTeSys (Cognition for Technical Systems)*².

REFERENCES

- [1] R. Arkin, R. Murphy, M. Pearson, and D. Vaughn, "Mobile robot docking operations in a manufacturing environment: Progress in visual perceptual strategies," in *Proceedings of the IEEE/RSJ International Workshop on Intelligent Robots and Systems*, 1989, pp. 147–154.
- [2] H. Hu and D. Gu, "Generalised predictive control of an industrial mobile robot," in *Proceedings of the IASTED International Conference on Intelligent Systems and Control*, 1999, pp. 235–240.
- [3] G. Alenya, J. Escoda, A. Martinez, and C. Torras, "Using laser and vision to locate a robot in an industrial environment: A practical experience," in *Proceedings of the IEEE International Conference on Robotics and Automation*, 2005, pp. 3528–3533.
- [4] A. Stopp, T. Baldauf, S. Horstmann, and S. Kristensen, "Dynamic work space surveillance for mobile robot assistants," in *Proceedings of the IEEE International Workshop on Robot and Human interactive Communication*, 2003, pp. 25–30.
- [5] M. Zäh, M. Beetz, K. Shea, G. Reinhard, K. Bender, C. Lau, M. Ostgathe, W. Vogl, M. Wiesbeck, M. Engelhard, C. Ertelt, T. Rühr, and M. Friedrich, *Changeable and Reconfigurable Manufacturing Systems*. Springer, 2009, ch. The Cognitive Factory, pp. 355–371.
- [6] Y. Yang and O. Brock, "Elastic roadmaps—motion generation for autonomous mobile manipulation," *Autonomous Robots*, vol. 28, no. 1, pp. 113–130, 2010.
- [7] W. Meeussen, M. Wise, S. Glaser, S. Chitta, C. McGann, P. Mihelich, E. Marder-Eppstein, M. Muja, V. Eruhimov, T. Foote, J. Hsu, R. B. Rusu, B. Marthi, G. Bradski, K. Konolige, B. P. Gerkey, and E. Berger, "Autonomous door opening and plugging in with a personal robot," in *Proceedings of the IEEE International Conference on Robotics and Automation*, 2010, pp. 729–736.
- [8] M. Silverman, B. Nies, D. and Jung, and G. Sukhatme, "Staying alive: A docking station for autonomous robot recharging," in *Proceedings of the IEEE International Conference on Robotics and Automation*, vol. 1, 2002, pp. 1050–1055.
- [9] R. Cassinis, F. Tampalini, P. Bartolini, and R. Fedrigotti, "Docking and charging system for autonomous mobile robots," University of Brescia, Tech. Rep. R.T.2005-02-4, 2005.
- [10] R. Luo, C. Liao, K. Su, and K. Lin, "Automatic docking and recharging system for autonomous security robot," in *Proceedings of the IEEE/RSJ International Conference on Intelligent Robots and Systems*, 2005, pp. 2953–2958.
- [11] R. Luo, C. Liao, and S. Lin, "Multi-sensor fusion for reduced uncertainty in autonomous mobile robot docking and recharging," in *Proceedings of the IEEE/RSJ International Conference on Intelligent Robots and Systems*, 2009, pp. 2203–2208.
- [12] C. McCarthy, N. Barnes, and R. Mahony, "A robust docking strategy for a mobile robot using flow field divergence," *IEEE Transactions on Robotics*, vol. 24, no. 4, pp. 832–842, 2008.
- [13] S. gon Roh, J. H. Park, Y. K. Song, K. Yang, M. Choi, H.-S. Kim, H. Lee, and H. R. Choi, "Flexible docking mechanism using combination of magnetic force with error-compensation capability," in *Proceedings of the IEEE International Conference on Automation Science and Engineering*, 2008, pp. 697–702.
- [14] Y.-C. Wu, M.-C. Teng, and Y.-J. Tsai, "Robot docking station for automatic battery exchanging and charging," in *Proceedings of the IEEE International Conference on Robotics and Biomimetics*, 2009, pp. 1043–1046.
- [15] S. gon Roh, J. H. Park, Y. H. Lee, Y. K. Song, K. W. Yang, M. Choi, H.-S. Kim, H. Lee, and H. R. Choi, "Flexible docking mechanism with error-compensation capability for auto recharging system of mobile robot," *International Journal of Control, Automation, and Systems*, vol. 6, no. 5, pp. 731–739, 2008.
- [16] S. Shoval, I. Zeitoun, and E. Lenz, "Implementation of a Kalman filter in positioning for autonomous vehicles, and its sensitivity to the process parameters," *The International Journal of Advanced Manufacturing Technology*, vol. 13, no. 10, pp. 738–746, 1997.
- [17] A. Balluchi, P. Souères, and A. Bicchi, "Hybrid feedback control for path tracking by a bounded-curvature vehicle," in *Proceedings of the International Workshop on Hybrid Systems: Computation and Control*, 2001, pp. 133–146.
- [18] G. Indiveri, A. Nüchter, and K. Lingemann, "High speed differential drive mobile robot path following control with bounded wheel speed commands," in *Proceedings of the IEEE International Conference on Robotics and Automation*, 2007, pp. 2202–2207.
- [19] A. Micaelli and C. Samson, "Trajectory tracking for unicycle-type and two-steering-wheels mobile robots," INRIA, Research Report RR-2097, 1993.
- [20] D. Soetanto, L. Lapierre, and A. Pascoal, "Adaptive, non-singular path-following control of dynamic wheeled robots," in *Proceedings of the IEEE Conference on Decision and Control*, vol. 2, 2003, pp. 1765–1770.
- [21] R. E. Kalman, "A new approach to linear filtering and prediction problems," *Transactions of the ASME—Journal of Basic Engineering*, vol. 82, no. Series D, pp. 35–45, 1960.

²<http://www.cotesys.org/>